Old Dominion University Research Foundation

DEPARTMENT OF AEROSPACE ENGINEERING
COLLEGE OF ENGINEERING AND TECHNOLOGY
OLD DOMINION UNIVERSITY
NORFOLK, VIRGINIA 23529

TRANSITION AND BREAKDOWN TO TURBULENCE IN INCOMPRESSIBLE BOUNDARY LAYER

By
Dr. Ponnampalam Balakumar, Principal Investigator

FINAL REPORT

For the period ending January 5, 1998

Prepared for
NASA Langley Research Center
Attn.: Mr. Joseph Murray
Grants Officer
Mail Stop 126
Hampton, VA 23681-0001

And

NASA Langley Research Center
Attn.: Mr. Ronald D. Joslin
Technical Officer
Mail Stop 170
Hampton, VA 23681-0001

Under
NASA Grant NAG1-1934
Research Title: PSE Computations in the Strongly Nonlinear Region
ODURF Project No. 172831

November 1998

DEPARTMENT OF AEROSPACE ENGINEERING
COLLEGE OF ENGINEERING AND TECHNOLOGY
OLD DOMINION UNIVERSITY
NORFOLK, VIRGINIA 23529

TRANSITION AND BREAKDOWN TO TURBULENCE IN INCOMPRESSIBLE BOUNDARY LAYER

By
Dr. Ponnampalam Balakumar, Principal Investigator

FINAL REPORT

For the period ending January 5, 1998

Prepared for
NASA Langley Research Center
Attn.: Mr. Joseph Murray
Grants Officer
Mail Stop 126
Hampton, VA 23681-0001

And

NASA Langley Research Center
Attn.: Mr. Ronald D. Joslin
Technical Officer
Mail Stop 170
Hampton, VA 23681-0001

Under
NASA Grant NAG1-1934
Research Title: PSE Computations in the Strongly Nonlinear Region
ODURF Project No. 172831

Submitted by
Old Dominion University Research Foundation
800 West 46th Street
Norfolk, VA 23508

November 1998

Transition and Breakdown to Turbulence in Incompressible Boundary Layers

P. Balakumar
Aerospace Engineering Department,
Old Dominion University, Norfolk, Virginia 23529–0247

Abstract

We have developed a code where the nonlinear terms are treated implicitly. The equations are discretized using the two-point fourth order compact scheme in the y-direction and the backward Euler method in the x-direction. We investigated the transition process in a Blasius boundary layer due to fundamental type breakdown. With 8 modes in the ω and β planes, we could compute the evolution of disturbances up to Re_x=910, which is well into the strongly nonlinear region. The transition onset point is located around Re_x=850. The comparison with the measurements and with the DNS computations are very good up to Re_x=880.

1. Introduction

Breakdown from laminar to turbulent flow in zero and mild pressure gradient boundary layers is caused by Tollmien-Schlichting (viscous) instability. Though there exist several mechanisms and routes to go from a laminar to a turbulent state, all of them in general follow these fundamental processes:

Receptivity

Linear instability

Nonlinear stability and saturation

Secondary instability

Breakdown to turbulence

In the receptivity process, the unsteadiness in the environment and the inhomogeneities in the geometry generate instability waves inside the flow. In quiet environments, the initial amplitudes of these instability waves are small compared to any characteristic velocity and length scales in the flow. Goldstein (1983 a) theoretically explained using asymptotic methods how the Tollmien-Schlichting waves (T-S waves) are generated near a leading edge of a flat plate by the long wavelength acoustic disturbances and in a companion paper (1985) described the scattering of T-S waves from the acoustic disturbances by the streamwise variations in surface geometries. In the second stage, the amplitudes of these instability waves grow exponentially downstream and this process is governed by the linearized Navier-Stokes equations. Further downstream, the amplitudes of the disturbances become large and the nonlinear effects inhibit the exponential growth and the amplitudes of the disturbances eventually saturate or attain singular values. In the next stage, these finite amplitude saturated disturbances become unstable to two- and/or three-dimensional disturbances. This is called secondary instability and beyond this stage the spectrum broadens, due to complex interactions and further instabilities, and the flow becomes turbulent in a short distance downstream. In this paper, we investigated the later stages of transition in Blasius boundary layers using Parabolized Stability Equations (PSE) approach.

The Parabolized Stability Equations (PSE) approach currently can predict the first three stages of the transition process, linear instability, nonlinear stability and saturation and secondary instability, accurately and very efficiently, Herbert (1997). After the skin friction rise the PSE computations cease to converge. There may be two sources for the program not to converge in this region. One is that the PSE approximation itself may not be valid in the highly nonlinear region. The other may be that the iteration on the nonlinear terms, at present they are treated explicitly and iterated till they converge, may not be converging. In this work, we will treat the nonlinear terms implicitly and will investigate how far downstream we can continue the PSE computations. If we can compute up to the skin friction maximum in the transition region, this will help us in developing new transition modeling and in developing improved transition prediction methods. We also observed that in some PSE computations, e.g., Gortler instability,

crossflow instability, at the later stages, the meanflow distortion term converges very slowly. Hence, in these cases the implicit formulation will improve the convergence.

2. Formulation

In the parabolized stability equations (PSE) approach, one attempts to construct an approximate solution of the full Navier-Stokes equations. The idea was first introduced by Herbert(1991) and applied to linear and non-linear Blasius boundary-layer flow by Bertolotti (1992). Now it has been developed and has been applied to two and three-dimensional incompressible and compressible boundary-layer flows (Chang et.al. 1994, Malik et.al 1994). Herbert (1997) in a recent review described the development and the application of PSE to different problems and here we give the governing equations and the procedure that we use to solve the equations.

We investigate the transition process in a Blasius boundary layer over a flat plate. Let us denote the Cartesian coordinate system by x_i (i=1,2,3), the velocity components by $\tilde{u}_i$ and the pressure by $\tilde{p}$. We decompose the total flow quantities as the sum of the mean flow and the disturbance quantities.

$$\begin{aligned} \tilde{u}_i(\mathbf{x},t) &= U_{0i}(\mathbf{x}) + u_i(\mathbf{x},t), \\ \tilde{p}_i(\mathbf{x},t) &= P_0(\mathbf{x}) + p_i(\mathbf{x},t), \end{aligned} \tag{1}$$

where, U_{0i} are the mean velocity components which are the solution of the Blasius equation and P is the mean pressure. Substituting these expressions into the Navier-Stokes equations we obtain the nonlinear equations for the disturbances in the form

$$\begin{aligned} \frac{\partial u_i}{\partial x_i} &= 0, \\ \frac{\partial u_i}{\partial t} + u_j\frac{\partial U_{0i}}{\partial x_j} + U_{0j}\frac{\partial u_i}{\partial x_j} + u_j\frac{\partial u_i}{\partial x_j} &= -\frac{\partial p}{\partial x_i} + \frac{1}{Re}\frac{\partial^2 u_i}{\partial x_j \partial x_j}, \end{aligned} \tag{2}$$

where the Reynolds number

$$Re = \frac{U_\infty L}{\nu}, \tag{3}$$

, U_∞ is the freestream velocity, and L is a reference length.

To derive the PSE equations, we write the dependent variables u_1, u_2, u_3, p as the sum of normal modes

$$q = \sum_{m=-MB}^{MB} \sum_{n=-MO}^{MO} q_{mn}(x_1, x_3) e^{i \int \alpha_{mn}(x_1) dx_1 + im\beta x_2 - in\omega t}. \tag{4}$$

Here ω is the frequency of the disturbance, β is the spanwise wave number, and $\alpha_{mn}(x_1)$ is the wave number in the axial direction. $q_{mn}(x_1, x_3)$ is the amplitude function for the mode (m,n) , MO is the total number of modes kept in the frequency domain in one quadrant and MB is the number of spanwise modes. Substituting this expression into the disturbance equations and making the PSE approximation, we obtain PSE equations for each mode (m,n).

$$\frac{\partial u_{3mn}}{\partial x_3} + i\alpha_{mn} u_{1mn} + im\beta u_{2mn} + \frac{\partial u_{1mn}}{\partial x_1} = 0. \tag{5}$$

$$\begin{aligned} \frac{\partial^2 u_{1mn}}{\partial x_3^2} =& \{Re\left(-in\omega + i\alpha_{mn} U_{01} + \frac{\partial U_{01}}{\partial x_1} + im\beta U_{02}\right) \\ &+ m^2\beta^2 + \alpha_{mn}^2 - i\frac{d\alpha_{mn}}{dx_1}\} u_{1mn} \\ &+ ReU_{03}\frac{\partial u_{1mn}}{\partial x_3} + Re\frac{\partial U_{01}}{\partial x_3} u_{3mn} + i\alpha_{mn} p_{mn} \\ &+ (ReU_{01} - 2i\alpha_{mn})\frac{\partial u_{1mn}}{\partial x_1} + Re\frac{\partial p_{mn}}{\partial x_1} \\ &+ Re\left\langle u_1\frac{\partial u_1}{\partial x_1} + u_2\frac{\partial u_1}{\partial x_2} + u_3\frac{\partial u_1}{\partial x_3}\right\rangle_{mn}. \end{aligned} \tag{6}$$

$$\begin{aligned} \frac{\partial^2 u_{2mn}}{\partial x_3^2} =& Re\frac{\partial U_{02}}{\partial x_1} u_{1mn} \\ &+ \{Re(-in\omega + i\alpha_{mn} U_{01} + im\beta U_{02}) \\ &+ m^2\beta^2 + \alpha_{mn}^2 - i\frac{d\alpha_{mn}}{dx_1}\} u_{2mn} \\ &+ ReU_{03}\frac{\partial u_{2mn}}{\partial x_3} + Re\frac{\partial U_{02}}{\partial x_3} u_{3mn} + im\beta p_{mn} \\ &+ (ReU_{01} - 2i\alpha_{mn})\frac{\partial u_{2mn}}{\partial x_1} \\ &+ Re\left\langle u_1\frac{\partial u_2}{\partial x_1} + u_2\frac{\partial u_2}{\partial x_2} + u_3\frac{\partial u_2}{\partial x_3}\right\rangle_{mn}. \end{aligned} \tag{7}$$

$$
\begin{aligned}
\frac{\partial p_{mn}}{\partial x_3} &= \left(-\frac{\partial U_{03}}{\partial x_1} + i\alpha_{mn}U_{03}\right)u_{1mn} \\
&+ U_{03} im\beta u_{2mn} \\
&+ \{in\omega - i\alpha_{mn}U_{01} - im\beta U_{02} - \frac{\partial U_{03}}{\partial x_3} \\
&+ \left(-m^2\beta^2 - \alpha_{mn}^2 + i\frac{d\alpha_{mn}}{dx_1}\right)\}u_{3mn} \\
&- \frac{i\alpha_{mn}}{Re}\frac{\partial u_{1mn}}{\partial x_3} - \frac{im\beta}{Re}\frac{\partial u_{2mn}}{\partial x_3} \\
&+ U_{03}\frac{\partial u_{1mn}}{\partial x_1} + \left(-U_{01} + \frac{2i\alpha_{mn}}{Re}\right)\frac{\partial u_{3mn}}{\partial x_1} \\
&- \frac{1}{Re}\frac{\partial^2 u_{1mn}}{\partial x_1 \partial x_3} \\
&- \left\langle u_1\frac{\partial u_3}{\partial x_1} + u_2\frac{\partial u_3}{\partial x_2} - u_3\frac{\partial u_1}{\partial x_1} - u_3\frac{\partial u_2}{\partial x_2}\right\rangle_{mn}.
\end{aligned}
\tag{8}
$$

At present, the nonlinear terms S_{mn} are evaluated from the values obtained at the previous iteration step and using the FFT technique. In the implicit formulation, these terms are function of$\tilde{Q}_{mn}$ and the system of equations becomes a set of coupled nonlinear equations. This nonlinear coupled equations will be solved using Newton - Raphson iteration technique Balakumar (1997).

3. Solution procedure

The eqs. (5–8) are solved using the two-point fourth order compact scheme, Malik et. al (1982), derived by means of the Euler-Maclaurin formula

$$
\begin{aligned}
\psi^k - \psi^{k-1} &= \frac{h_k}{2}\left(\frac{d\psi^k}{dY} + \frac{d\psi^{k-1}}{dY}\right) - \frac{h_k^2}{12}\left(\frac{d^2\psi^k}{dY^2} + \frac{d^2\psi^{k-1}}{dY^2}\right) \\
&+ O(h_k^5),
\end{aligned}
\tag{9}
$$

where, $\psi^k = \psi(Y_k)$ and $h_k = Y_k - Y_{k-1}$.

To apply the above scheme to this problem, we have to rewrite eqs. (5–8) as a system of first order equations. The eqs. (5–8) can easily be written as

$$
\psi'_{n,m} = F_{n,m}(\psi, Y) \quad n = -MB \text{ to } MB, \quad m = -MO \text{ to } MO, \tag{10}
$$

where, $\psi = \left\{ \psi^T_{-MB,-MO}, \ldots, \psi^T_{MB,MO} \right\}$ and $\psi_{n,m} = \left\{ u_{n,m}, u'_{n,m}, w_{n,m}, w'_{n,m}, v_{n,m}, p_{n,m} \right\}^T$.

$\psi_{n,m}$ and $F_{n,m}$ are (6 x 1) complex column vectors and ψ is a (6 x (2*MB* + 1)*(2*MO* + 1)) complex column vector. From eq. (10), we get

$$\psi''_{n,m} = \frac{\partial F}{\partial Y} + \left\{ \frac{\partial F_{n,m}}{\partial \psi} \right\} F, \tag{11}$$

where, $F = \left\{ F^T_{-MB,-MO}, \ldots, F^T_{MB,MO} \right\}$. Substituting eqs. (10) and (11) into (9), we obtain

$$\begin{aligned} &\psi^k_{n,m} - \psi^{k-1}_{n,m} = \frac{h_k}{2}\left(F^k_{n,m} + F^{k-1}_{n,m} \right) \\ &- \frac{h_k^2}{12}\left(F'^k_{n,m} + \left(\frac{\partial F_{n,m}}{\partial \psi} \right)^k F^k - F'^{k-1}_{n,m} - \left(\frac{\partial F_{n,m}}{\partial \psi} \right)^{k-1} F^{k-1} \right) \\ &\text{for } n = -MB \text{ to } MB, \ m = -MO \text{ to } MO \text{ and } k = 2, N+1, \end{aligned} \tag{12}$$

where, $N + 1$ is the total number of grid points in the normal direction. This is a system of non-linear algebraic equations which is solved using the Newton-Raphson iterative method. We write $\psi_{n,m} = \psi_{on,m} + \Delta\psi_{n,m}$ and substitute into the eq. (12) and linearize in $\Delta\psi$, to obtain

$$\begin{aligned} &\psi^k_{on,m} + \Delta\psi^k_{n,m} - \psi^{k-1}_{on,m} - \Delta\psi^{k-1}_{n,m} \\ &= \frac{h_k}{2}\left(F^k_{on,m} + F^{k-1}_{on,m} + \left(\frac{\partial F_{on,m}}{\partial \psi} \right)^k \Delta\psi^k + \left(\frac{\partial F_{on,m}}{\partial \psi} \right)^{k-1} \Delta\psi^{k-1} \right) \\ &- \frac{h_k^2}{12}\left\{ F'^k_{on,m} + \left(\frac{\partial F'_{on,m}}{\partial \psi} \right)^k \Delta\psi^k + \left(\frac{\partial F_{on,m}}{\partial \psi} \right)^k F^k \right. \\ &+ \left(\frac{\partial F_{on,m}}{\partial \psi} \right)^k \left(\frac{\partial F_{on,m}}{\partial \psi} \right)^k \Delta\psi^k + \left(\frac{\partial^2 F_{on,m}}{\partial \psi^2} \right) \\ &- F'^{k-1}_{on,m} - \left(\frac{\partial F'_{on,m}}{\partial \psi} \right)^{k-1} \Delta\psi^k - \left(\frac{\partial F_{on,m}}{\partial \psi} \right)^{k-1} F^{k-1}_o \\ &- \left(\frac{\partial F_{on,m}}{\partial \psi} \right)^{k-1} \left(\frac{\partial F_{on,m}}{\partial \psi} \right)^{k-1} \Delta\psi^{k-1} - \left(\frac{\partial^2 F_{on}}{\partial \psi^2} \right)^{k-1} \\ &\left. F^{k-1}_o \Delta\psi^{k-1} \right\} \\ &\text{for } n = 0, MB, \ m = 0, MO, \text{ and } k = 2, N+1. \end{aligned} \tag{13}$$

Collecting the terms we obtain a linear system of equations for $\Delta\psi^k$ and $\Delta\psi^{k-1}$ which can be written as

$$A_k \Delta\psi^{k-1} + B_k \Delta\psi^k = D_k \qquad \text{for } k = 2, N+1, \tag{14}$$

where A_k, B_k are complex matrices of size ((MB + 1)x(MO+1) x 6, (2MB + 1)x(2MO+1) x 6) and D_k is a complex vector of size (MB + 1)x(MO+1) x 6. Using the property $\Delta\psi_{n,m} = \Delta\psi^*_{-n,-m}$ $\Delta\psi_{n,m} = \Delta\psi_{-n,m}$ (where * stands for complex conjugate), we can rewrite this equation in real and imaginary parts of $\Delta\psi_{n,m}(n = 0, ..., MB,\ m = 0, ..., MO)$.

$$\bar{A}_k \begin{Bmatrix} \Delta\psi_r \\ \Delta\psi_i \end{Bmatrix}^{k-1} + \bar{B}_k \begin{Bmatrix} \Delta\psi_r \\ \Delta\psi_i \end{Bmatrix}^{k} = \bar{D}_k, \qquad k = 2, (N+1), \tag{15}$$

where $\bar{A}_k$, $\bar{B}_k$ are real matrices of size (MB + 1)x(MO+1) x 12. The boundary conditions can be written as,

$$\bar{B}_1 \begin{Bmatrix} \Delta\psi_r \\ \Delta\psi_i \end{Bmatrix}^{1} = \bar{D}_1, \tag{16}$$

and

$$\bar{A}_{N+2} \begin{Bmatrix} \Delta\psi_r \\ \Delta\psi_i \end{Bmatrix}^{N+1} = \bar{D}_{N+2}, \tag{17}$$

where, $\bar{B}_1$ and $\bar{A}_{N+2}$ are ((MB + 1)x(MO+1) x 6, (MB + 1)x(MO+1) x 12) real matrices and $\bar{D}_1$, $\bar{D}_{N+2}$ are ((MB + 1)x(MO+1) x 6) column vectors. Combining eqs. (15–17) we can form a block tridiagonal system or can write it as a banded system, both of which can be solved very efficiently.

4. Computational efficiency

In order to discuss the efficiency and the robustness of the implicit solution method in comparison with the explicit method, this section will show results from an application of both methods to the Swept Hiemenz flow problem. Relevant parameters and the mean flow profiles are given in Malik, Fei and Chang (1996). For a Reynolds number in the spanwise direction of $\overline{Re_0} = 500$, a steady disturbance with a spanwise wave number of $\beta_1 = 0.4$ and an initial amplitude of A=0.1% is introduced at the streamwise position of $Re_0 = 150$.

Figure 1 shows the growth rates σ_1 based on the disturbance component in the spanwise direction that are obtained from the explicit and the implicit method. Additionally, the linear growth rates are plotted. Besides the perfect agreement of the results obtained from the different methods, it is noted that the nonlinear effects modify the growth rate starting at a Reynolds number of Re=400. It is further seen that the explicit method ceases to converge at Re=570 for an SUR-parameter (Successive Under Relaxation) of 1.0., whereas the implicit method continues to converge well beyond the plotted region. It is noted that a Reynolds number of Re=570 corresponds to the region where the stationary disturbances saturate, and hence, the nonlinear effects are indeed strong at the point where the explicit method stops converging for an SUR-parameter of 1.0.

The number of iterations on the nonlinear terms necessary to obtain converged solution, and the convergence history at Re=570 are shown in figures 2 and 3, respectively. There, the residue is defined as the maximal difference in the shape functions of the primary disturbance obtained in two consecutive iterations. The extremely rapid convergence of the implicit method is visualized in the figure 3 and shows the superiority of the implicit method in the developed nonlinear region.

Two observations can be made from these plots. First, in the region of linear disturbance growth (Re<400), the explicit method needs as many iterations on the nonlinear terms as the implicit method. Since the explicit method iterates just on the primary disturbance, whereas the implicit method computes all disturbances simultaneously, the explicit method is expected to be much more efficient in that region. With an increasing effect of the nonlinear terms for Re>400,

however, this similar performance of the two methods is altered significantly. The number of iterations on the nonlinear terms using the explicit method increases exponentially, whereas the performance of the implicit code basically remains unchanged.

It is concluded that the implicit method provides a powerful tool to conduct nonlinear PSE computations in the regions of highly nonlinear disturbance growth. The most effective technique in applying the developed algorithms is seen in combining the explicit and implicit methods by starting the computations with the explicit method, and once a critical number of nonlinear iterations is reached, by continuing with the implicit method.

5. Transition due to Klebanoff type breakdown

Next we investigated the transition process in the Blasius boundary layer due to fundamental breakdown process (K-type). We simulated one of the experiments performed by Saric et al. (1981) and the parameters are given in Table 1.

$$\begin{aligned} F &= .76 * 10^{-4} \\ \beta &= .142 \\ Re_0 &= 710 \\ (u_{0,1})_{max} &= .00338 \\ (u_{1,1})_{max} &= .00024 \end{aligned} \tag{18}$$

Here, the variables are nondimensionalised by

$$\begin{aligned} &\text{velocity : Free stream velocity } U_\infty \\ &\text{length : } \sqrt{\frac{\nu x_0}{U_\infty}}. \end{aligned} \tag{19}$$

Here, F is the non-dimensional frequency frequency defined by

$$F = \frac{2\pi\nu f}{U_\infty^2}, \tag{20}$$

and Re_0 is the Reynolds number at the initial location $x=x_0$. The Reynolds numbers Re_x, RE_x and the skin friction coefficient c_f are defined by

$$Re_x = \sqrt{\frac{U_\infty x}{\nu}}$$
$$RE_x = \frac{U_\infty x}{\nu} \tag{21}$$
$$c_f = \frac{\tau_w}{\rho U_\infty^2}.$$

Figure 4 shows the variation of the maximum rms fluctuations for the streamwise velocity with the Reynolds number. The results are compared with the experimental results of Saric et. al. (1984) and with the DNS results of Liu et. al. (1995). We used 8 and 12 modes, MB=MO=8, 12 in these computations. With the SUR parameter (Successive under relaxation) equals to 1.0, the explicit code ceases to converge beyond Re_x=860, and with SUR=.25, we can extend the computations up to Re_x=880 and with the implicit code up to Re_x=905 with 8 modes. With the 12 modes, the explicit code stops converging at Re_x=880 and we did not have enough memory in the computer to continue further using the implicit code. It is seen that the computed results are in good agreement with the experiment and with the DNS results.

Figure 5 shows the distribution of u_{rms} in the y-direction at different axial locations Re_x=855, 865, 875, 885 and 890. Re_x=855 is approximately the transition onset point. We observe that the location where u_{rms} peaks increases with the downstream direction. This is in good qualitative agreement with the Klebanoff et. al. (1961) measurements.

Figure 6 shows the variation of the skin friction coefficient c_f with the Reynolds number. For comparison, we also plotted the skin friction coefficient for the Blasius boundary layer. We note that the transition onset point is located at Re_x=855 and beyond this point skin friction increases sharply. These results show that we can compute the transition process in the fully nonlinear region using PSE approach. In figure 7, we plotted the modified mean velocity profile and the unmodified Blasius boundary layer profile at Re_x=890. It is seen that the velocity increases in

the region close to the wall and decreases in the outer part of the boundary layer. Hence the boundary layer profiles gradually become fuller in the fully nonlinear region.

In figure 8, we plotted the variation of unsteady u fluctuations at the maximum rms locations with time at different Reynolds numbers. The results show that up to Re_x=875, the oscillations are approximately sinusoidal and beyond this stage the disturbances have smaller positive amplitude and larger negative value. At Re_x=890, the maximum positive value is about 0.1 and the minimum value is –0.2. Hence it shows that the evolution of the disturbances approach 1 "spike" stage according to Klebanoff et. al. (1961).

In figures 9(a-i) we plotted the evolution of different modes in the streamwise direction. Each figure shows the results for at a fixed $m\omega$ for different $n\beta$ where n=0 to 8. Figure 9(a) shows the results for MO=0 and figure 9(i) depicts the results for MO=9. First observation is that the amplitude of the disturbances gradually decreases with increasing $m\omega$. Up to this Reynolds number Re_x= 890, the important modes are the steady waves MO= 0 and the fundamental wave MO=1. Second observation is that beyond the secondary instability region, the disturbances saturate and there is no explosive growth nor any instability of the disturbances. This agrees with the DNS computations of Krist and Zang (1987).

6. Conclusions

We have developed a PSE code where the nonlinear terms are treated implicitly. The equations are discretized using two-point fourth order compact scheme in the y-direction and the backward Euler method in the x-direction. We investigated the transition process in a Blasius boundary layer due to fundamental type breakdown. With the 8 modes in ω and β planes, we could compute the evolution of disturbances up to Re_x=910, which is well into the strongly nonlinear region. The transition onset point is located around Re_x=850. The comparison with the measurements and with the DNS computations are very good up to Re=880.

In future, we have to repeat this computations with larger number of modes. This will require large memory and may not be possible to increase the modes beyond a limit. One solution is

to look for efficient iterative schemes to solve the coupled equations. Secondly, we have to perform the computations for several different cases to conclude the effectiveness of the PSE approach in the fully nonlinear region.

Acknowledgement

The computations are performed on the SUN workstations at ICASE/NASA Langley Research Center in Hampton, Virginia.

References

1. Balakumar, P., 1997 Finite-amplitude equilibrium solutions for Poiseuille-Couette flow. Theoret. Comput. Fluid Dynamics 9, 103–119.
2. C. L. Chang and M. R. Malik, "Oblique-mode breakdown and secondary instability in supersonic boundary layers," J. Fluid Mech. 273:323–360, 1994
3. M. E. Goldstein, "Scattering of acoustic waves into Tollmien-Schlichting waves by small streamwise variations in surface geometry," J. Fluid Mech. 154:509–529, 1985.
4. M. E. Goldstein, "Scattering of acoustic waves into Tollmien-Schlichting waves by small streamwise variations in surface geometry," J. Fluid Mech. 154:509–529, 1985.
5. F. Bertolotti, T. Herbert and P. Spalart, "Linear and Nonlinear stability of the Blasius boundary layer," J. Fluid Mech. 242:441–474, 1992.
6. T. Herbert , "Parabolized stability equations," Annual Review of Fluid Mechanics, 29, 245–283, 1997.
7. T. Herbert , "Boundary layer transition – analysis and prediction revisited," AIAA paper 91–0737, 1991.
8. P. S. Klebanoff, K. D. Tidstrom and L. M. Sargent, "The three-dimensional nature of boundary-layer instability", J. Fluid Mech. 12: 1-34, 1961.
9. S. E. Krist and T. A. Zang, " Numerical Simulation of Channel Flow Transition", NASA Technical Paper 2667. 1987.
10. C. Liu and Z. Liu, "Multigrid Mapping and Box Relaxation for Simulation of the Whole Process of Flow Transition on 3D Boundary Layers." J. Comput. Phys. 119, 325–341, 1995.
11. M. R. Malik, S. Chuang, and M. Y. Hussaini. "Accurate numerical solution of compressible, linear stability equations. "*Journal of Applied Mathematics and Physics*, 33(2):189-201, March 1982.
12. M. R. Malik, F. Li, and C. L. Chang , "Crossflow disturbances in three-dimensional boundary layers; Nonlinear development, wave interaction and secondary instability," J. Fluid Mech. 268:1–36, 1994.

13. W. S. Saric, V. V. Kozlov, and C. Ya. Levchenko, " Forced and Unforced Subharmonic Resonance in Boundary-Layer Transition", AIAA Paper No. 84–0007, 1984.

List of Figures

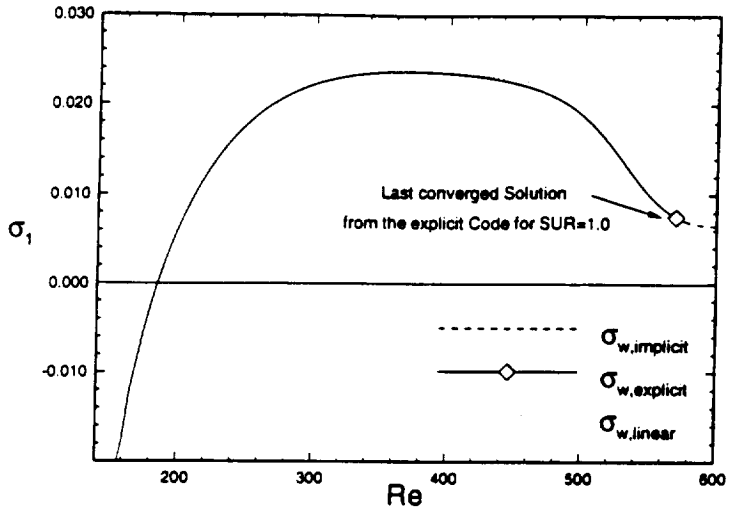

Figure 1. Growth rates and regions of convergence for the explicit and the implicit methods.

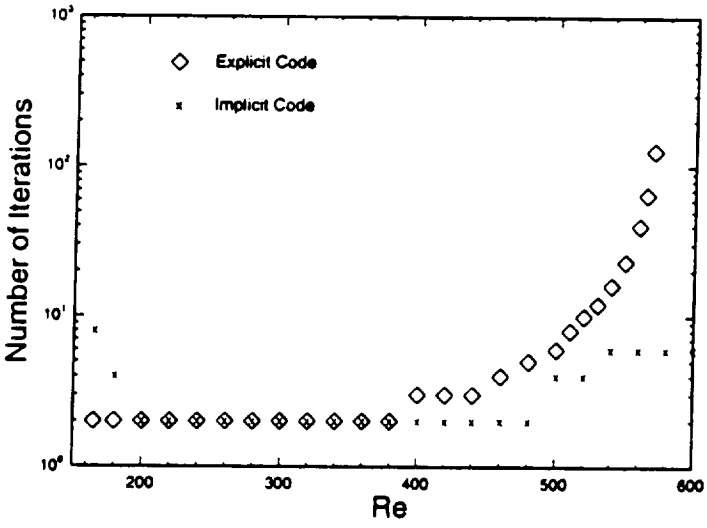

Figure 2. Number of iterations on the nonlinear terms (SUR=1.)

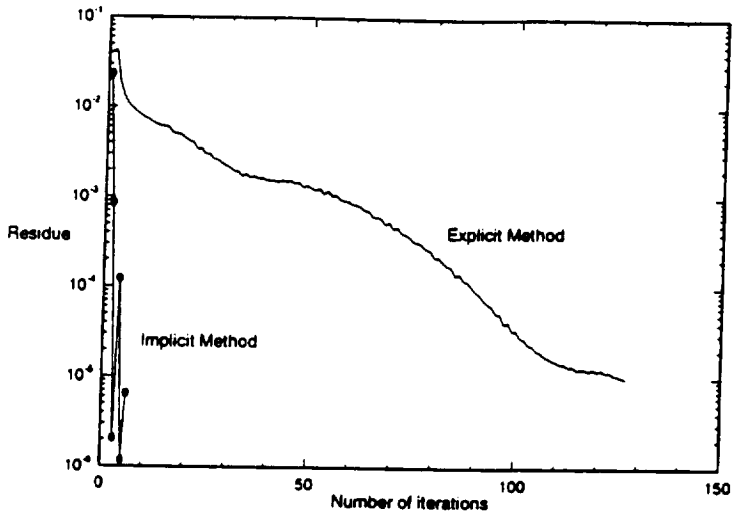

Figure 3. Convergence history for the explicit and the implicit methods at Re=570 (SUR=1.)

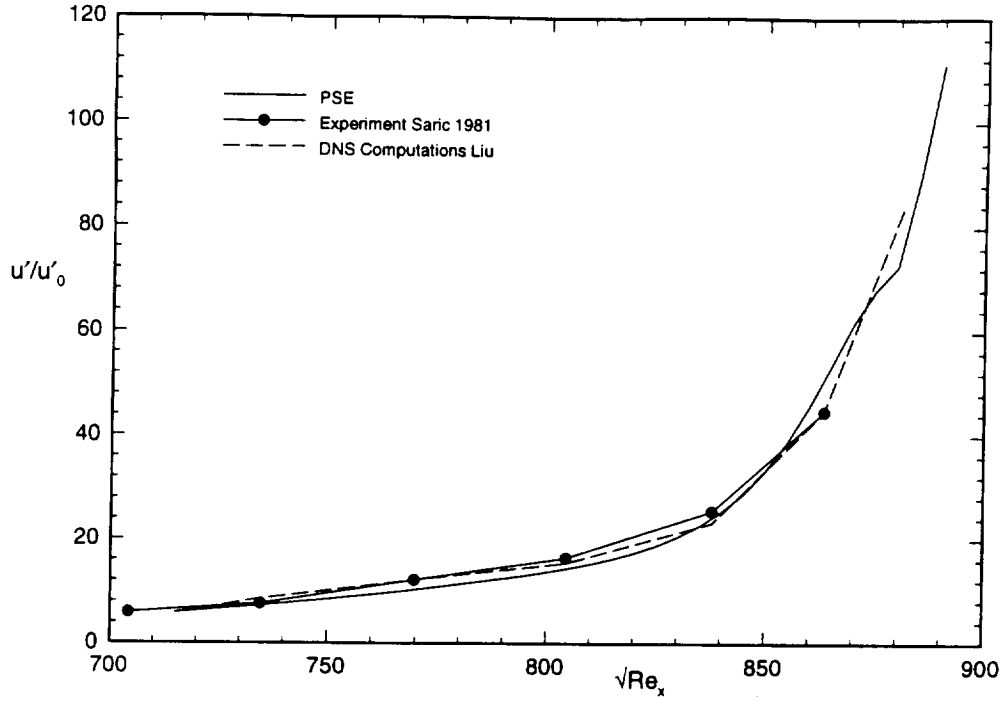

Figure 4. Variation of the amplitude of the axial velocity in the axial direction.

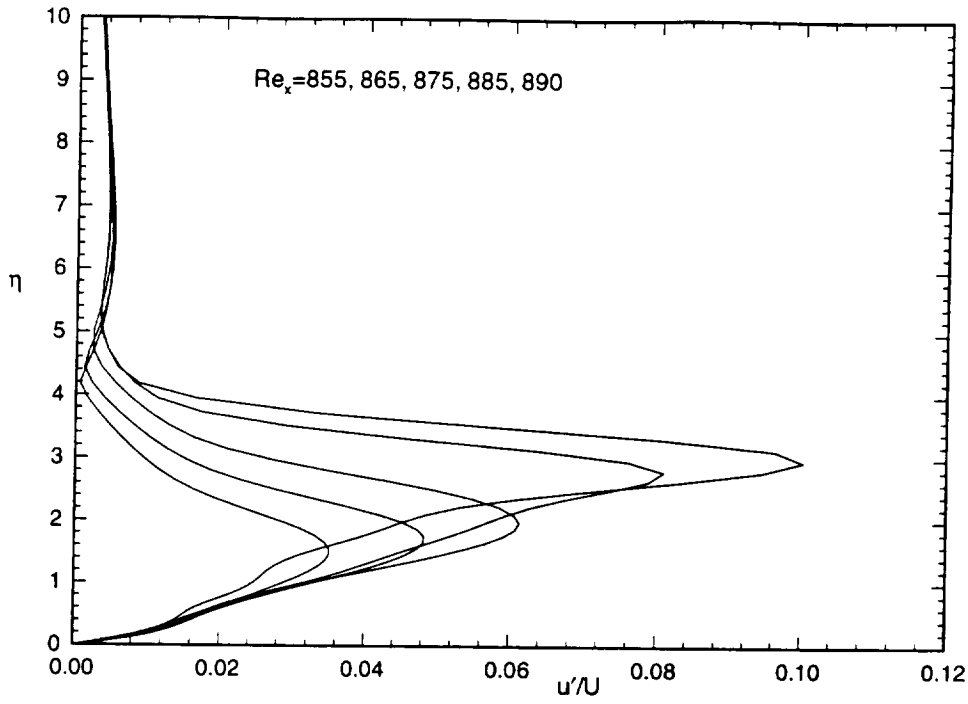

Figure 5. Distribution and evolution of the rms value of the axial velocity.

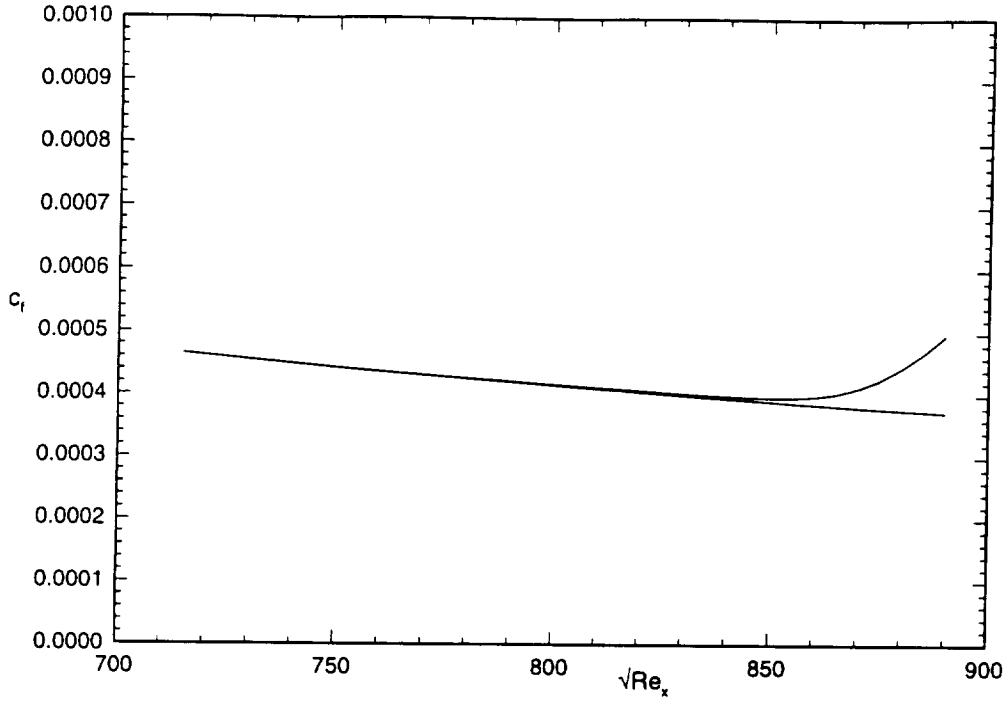

Figure 6. Variation of the skin friction coefficient in the axial direction.

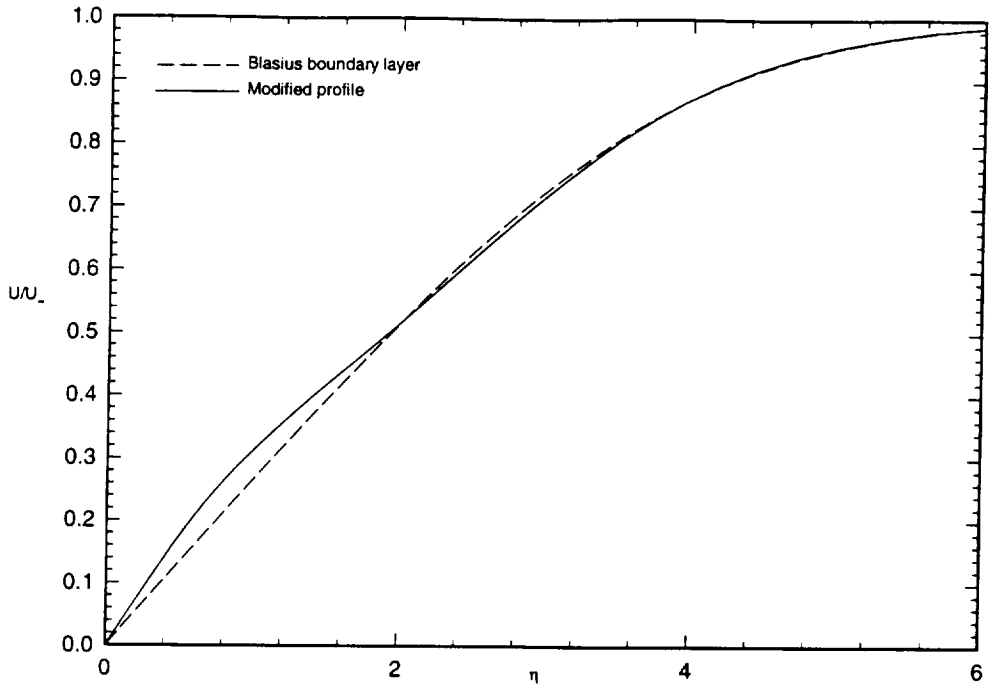

Figure 7. Modified mean velocity profiles at different axial locations.

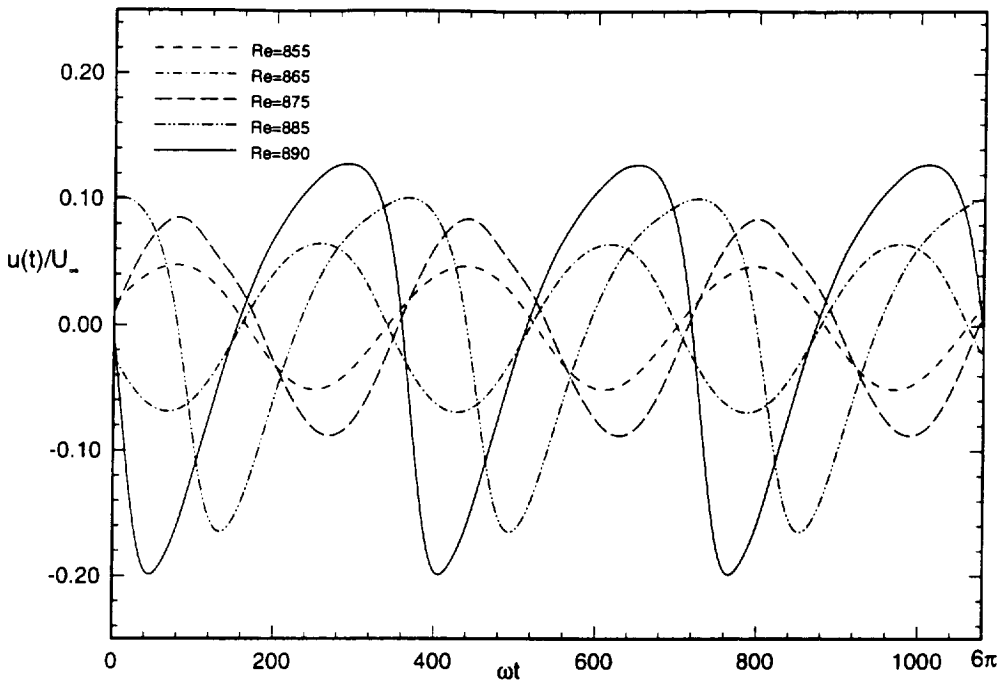

Figure 8. Fluctuations of axial velocity with time at the maximum rms locations and at different axial locations.

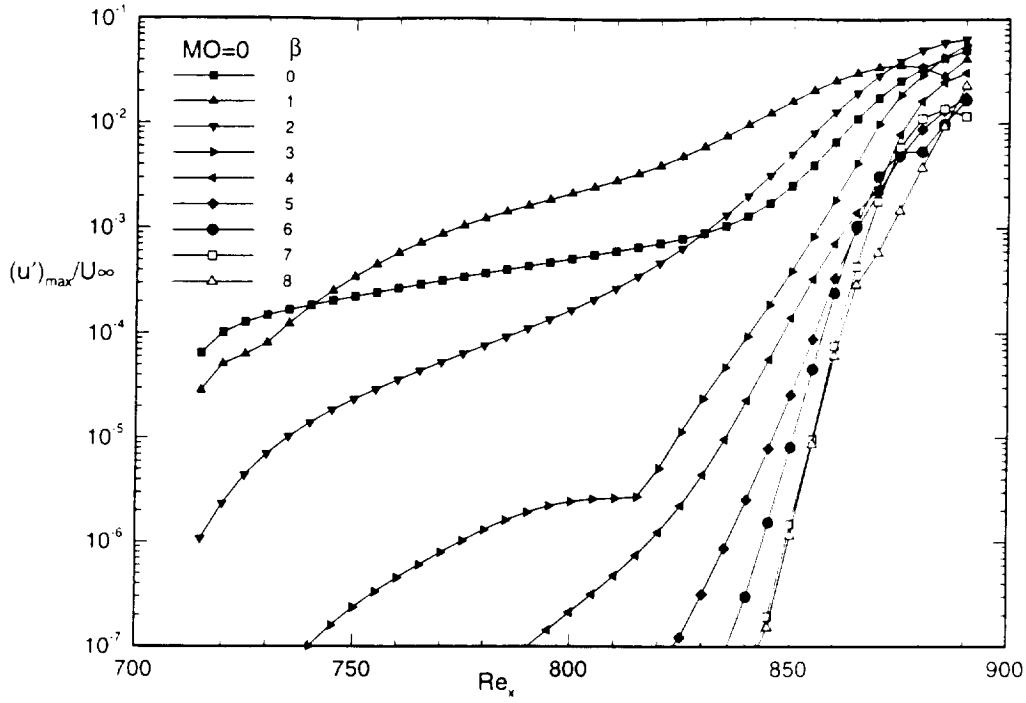
MO=0
β
0
1
2
3
4
5
6
7
8
10^{-1}
10^{-2}
10^{-3}
10^{-4}
10^{-5}
10^{-6}
10^{-7}
$(u')_{max}/U\infty$
700
750
800
850
900
Re_x

Figure 9(a).

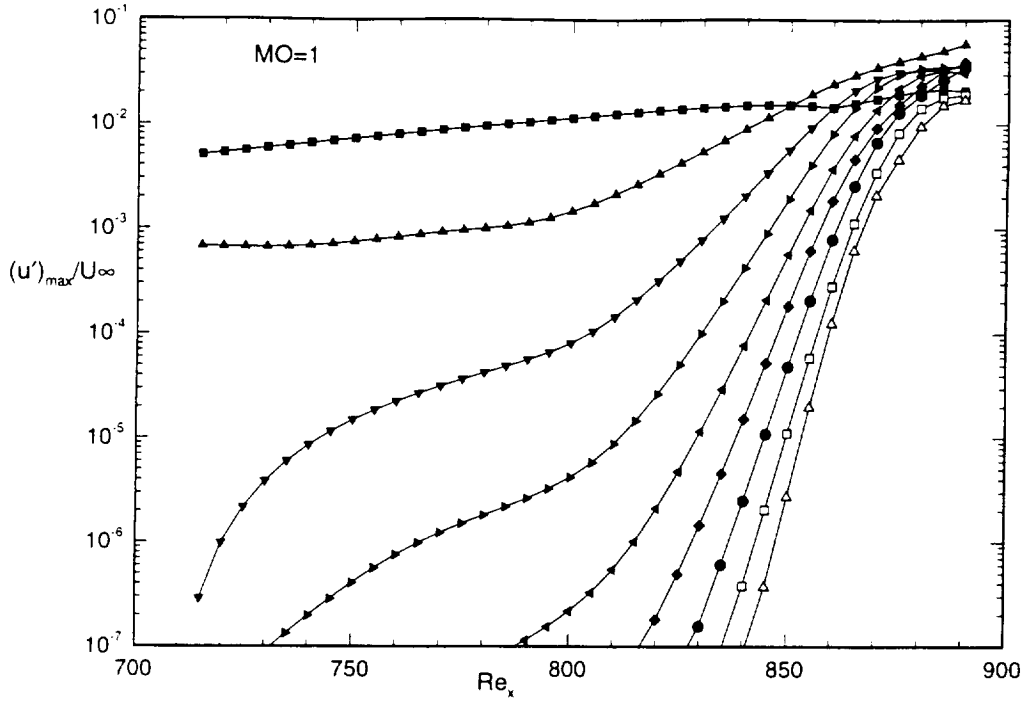
MO=1
10^{-1}
10^{-2}
10^{-3}
10^{-4}
10^{-5}
10^{-6}
10^{-7}
$(u')_{max}/U_\infty$
700
750
800
850
900
Re_x

Figure 9(b).

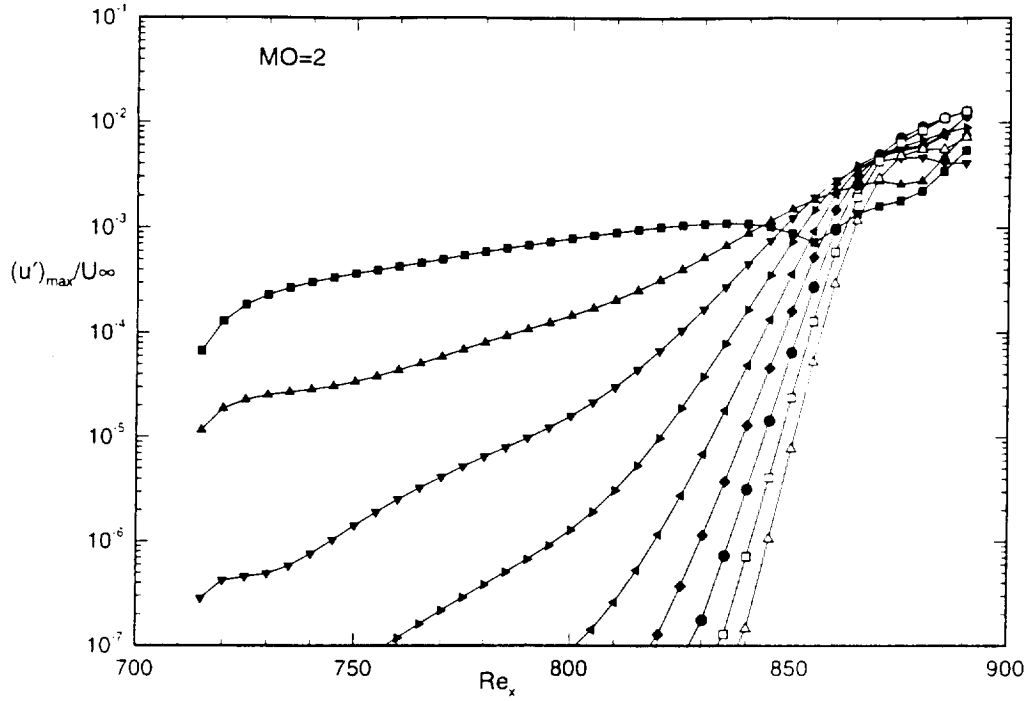
MO=2
10^{-1}
10^{-2}
10^{-3}
10^{-4}
10^{-5}
10^{-6}
10^{-7}
$(u')_{max}/U_\infty$
700
750
800
850
900
Re_x

Figure 9(c).

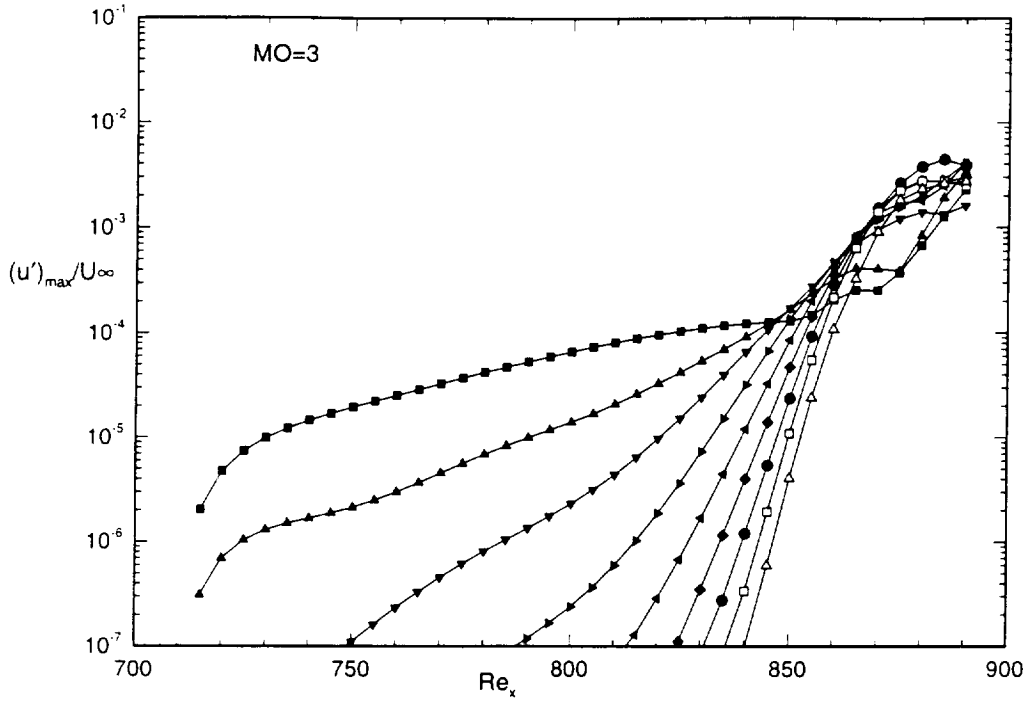
MO=3
10^{-1}
10^{-2}
10^{-3}
10^{-4}
10^{-5}
10^{-6}
10^{-7}
$(u')_{max}/U_\infty$
700
750
800
850
900
Re_x

Figure 9(d).

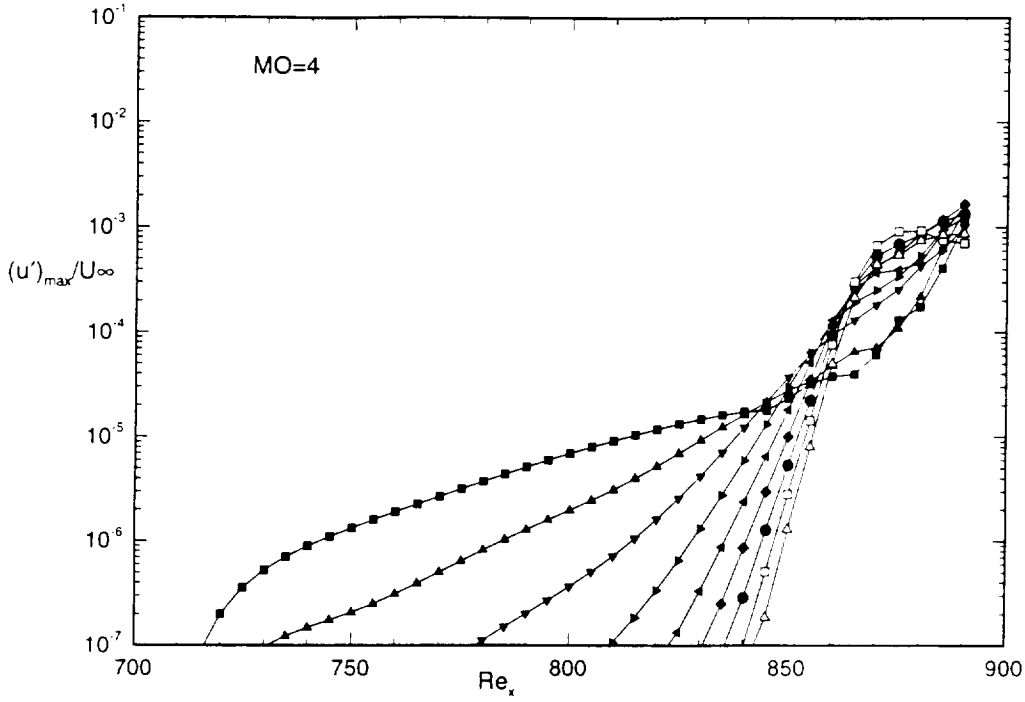
MO=4
10^{-1}
10^{-2}
10^{-3}
10^{-4}
10^{-5}
10^{-6}
10^{-7}
$(u')_{max}/U_\infty$
700
750
800
850
900
Re_x

Figure 9(e).

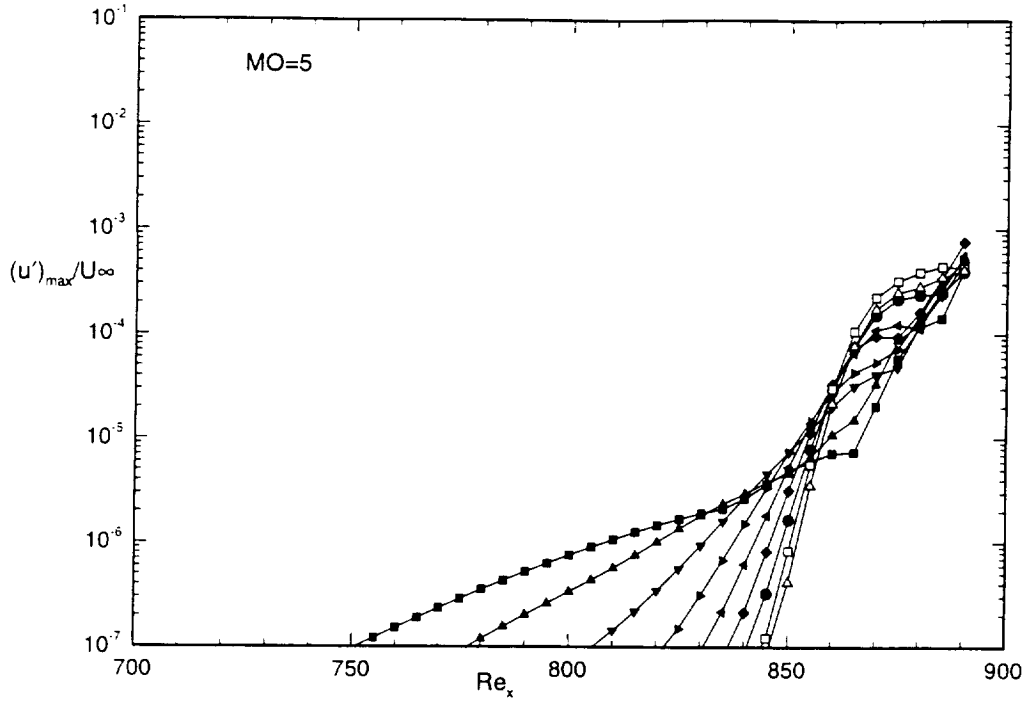
MO=5
10^{-1}
10^{-2}
10^{-3}
10^{-4}
10^{-5}
10^{-6}
10^{-7}
$(u')_{max}/U_\infty$
700
750
800
850
900
Re_x

Figure 9(f).

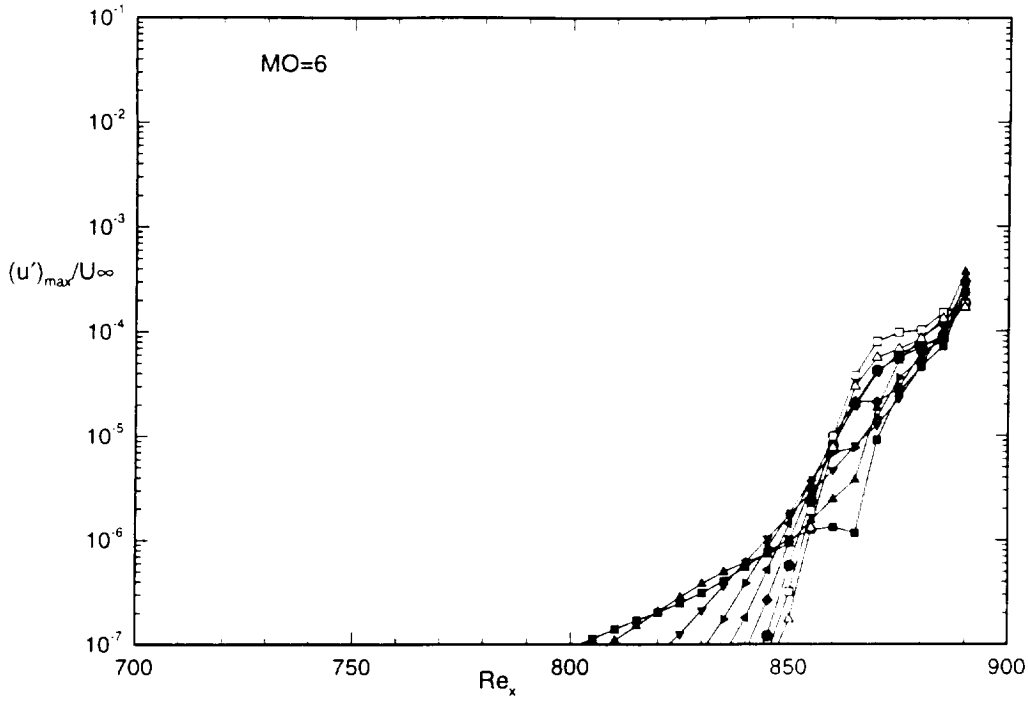
MO=6
10^{-1}
10^{-2}
10^{-3}
10^{-4}
10^{-5}
10^{-6}
10^{-7}
$(u')_{max}/U_\infty$
700
750
800
850
900
Re_x

Figure 9(g).

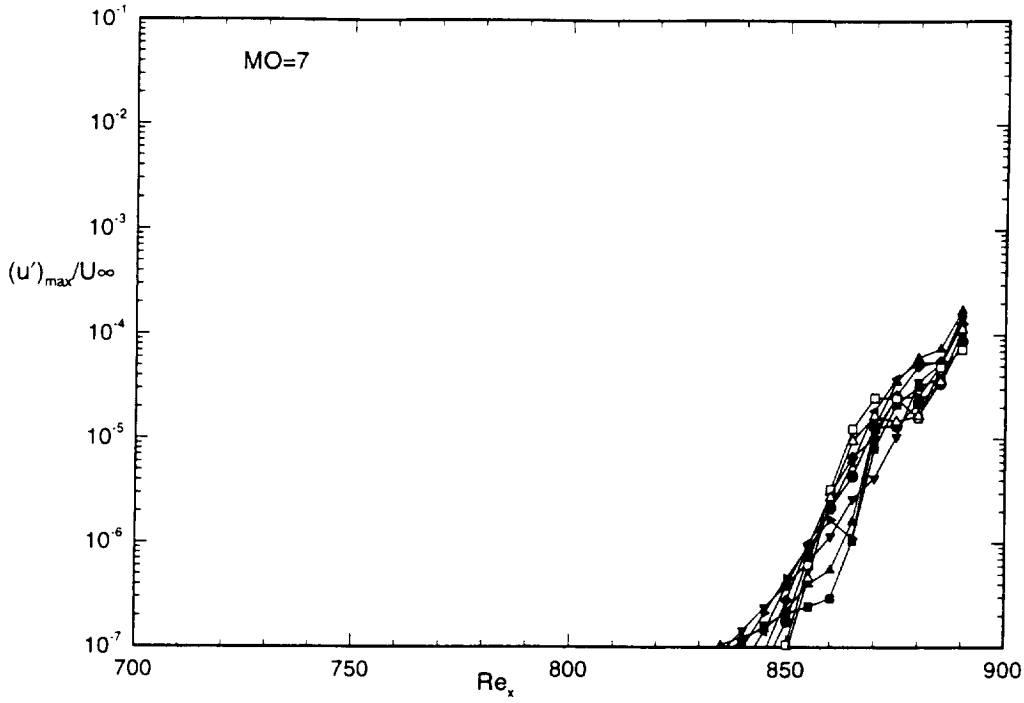
MO=7
10^{-1}
10^{-2}
10^{-3}
10^{-4}
10^{-5}
10^{-6}
10^{-7}
$(u')_{max}/U_\infty$
700
750
800
850
900
Re_x

Figure 9(h).

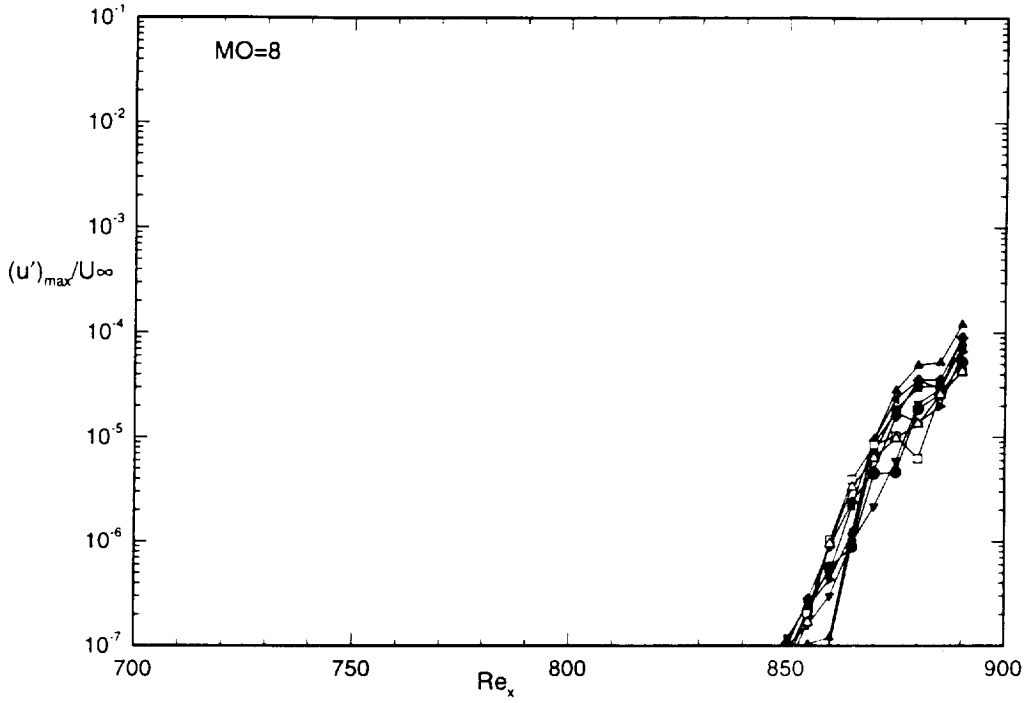

Figure 9(a-i). Evolution of the maximum amplitudes of different modes.